

Effects of rotational disruption on the evolution of grain size distribution in galaxies

Hiroiyuki Hirashita¹^{*} and Thiem Hoang^{2,3}

¹*Institute of Astronomy and Astrophysics, Academia Sinica, Astronomy-Mathematics Building, AS/NTU, No. 1, Sec. 4, Roosevelt Road, Taipei 10617, Taiwan*

²*Korea Astronomy and Space Science Institute, Daejeon 34055, Republic of Korea*

³*Korea University of Science and Technology, 217 Gajeong-ro, Yuseong-gu, Daejeon 34113, Republic of Korea*

Accepted XXX. Received YYY; in original form ZZZ

ABSTRACT

Interstellar dust grains can be spun up by radiative torques, and the resulting centrifugal force may be strong enough to disrupt large dust grains. We examine the effect of this rotational disruption on the evolution of grain size distribution in galaxies. To this goal, we modify our previous model by assuming that rotational disruption is the major small-grain production mechanism. We find that rotational disruption can have a large influence on the evolution of grain size distribution in the following two aspects especially for composites and grain mantles (with tensile strength $\sim 10^7$ erg cm⁻³). First, because of the short time-scale of rotational disruption, the small-grain production occurs even in the early phase of galaxy evolution. Therefore, even though stars produce large grains, the abundance of small grains can be large enough to steepen the extinction curve. Secondly, rotational disruption is important in determining the maximum grain radius, which regulates the steepness of the extinction curve. For compact grains with tensile strength $\gtrsim 10^9$ erg cm⁻³, the size evolution is significantly affected by rotational disruption only if the radiation field is as strong as (or the dust temperature is as high as) expected for starburst galaxies. For compact grains, rotational disruption predicts that the maximum grain radius becomes less than 0.2 μ m for galaxies with a dust temperature $\gtrsim 50$ K.

Key words: dust, extinction – galaxies: evolution – galaxies: high-redshift – galaxies: ISM – galaxies: starburst – radiation: dynamics

1 INTRODUCTION

Dust grains are known to be important for various processes in the interstellar medium (ISM) and galaxies. Many of the important processes concern the surface area of dust grains. Some molecules such as H₂ form on dust surfaces (e.g. Gould & Salpeter 1963; Cazaux & Tielens 2004); thus, their reaction rates are governed by the grain surface area, which is determined by the grain size distribution (distribution function of grain radius) (Hirashita & Harada 2017; Chen et al. 2018). Dust grains also interact with radiation by absorbing stellar ultraviolet (UV)–optical light and reprocess it in the infrared. This means that dust modifies or even governs the spectral energy distributions (SEDs) of galaxies (e.g. Takeuchi et al. 2005a). The cross-section of a dust grain for absorption and scattering (i.e. extinction), whose wavelength dependence is referred to as the extinction curve, depends on the grain size distribution (e.g. Mathis et al. 1977,

hereafter MRN). Thus, the evolution of grain size distribution is of fundamental importance in understanding the chemical and radiative processes in the ISM and galaxies.

There have been some studies modelling and calculating the evolution of grain size distribution in the ISM. Liffman & Clayton (1989) traced the size evolution of individual dust grains, considering dust destruction by supernova (SN) shocks and dust growth by accretion. This method is useful, for example, to derive the lifetime of dust as a function of grain radius, but the interactions between grains are not easy to include. O’Donnell & Mathis (1997) modelled the grain size distribution by further considering collisional processes (coagulation and shattering) in a multiphase ISM and showed that the extinction curves calculated from the resulting grain size distributions broadly reproduce the Milky Way extinction curve. The evolution of grain size distribution was first modelled in a consistent manner with the chemical enrichment of galaxies by Yamasawa et al. (2011). They took into account dust formation and destruction by SNe. In addition to these processes, Asano et al. (2013) com-

* E-mail: hirashita@asiaa.sinica.edu.tw

pleted the model by additionally including dust formation by AGB stars, dust growth by accretion and coagulation, and dust disruption by shattering. Nozawa et al. (2015) applied this model to high-redshift quasars, and showed that the calculated grain size distribution explains the observed extinction curve in a $z = 6.2$ quasar (z is the redshift). The evolution model of grain size distribution has been further combined with hydrodynamic simulations by post-processing (Hirashita & Aoyama 2019; Rau et al. 2019) or by a direct implementation (McKinnon et al. 2018; Aoyama et al. 2020). Hirashita & Murga (2020, hereafter HM20) used a one-zone galaxy model but further decomposed the calculated grain size distribution into relevant species (silicate and aromatic/non-aromatic carbon). Their model is also consistent with the abundance of polycyclic aromatic hydrocarbons (PAHs) in nearby galaxies (see also Seok et al. 2014).

In the above, shattering is the unique mechanism that creates small grains efficiently. Recently, Hoang (2019) has proposed another mechanism of creating small grains from large grains – rotational disruption (see also Hoang et al. 2019). In the presence of strong radiation, grains acquire suprathermal rotation driven by radiative torques (Draine & Weingartner 1996; Hoang & Lazarian 2008, 2009). This rotation induces the centrifugal stress in the dust grain. Hoang et al. (2019) found that large dust grains can be disrupted because the centrifugal stress exceeds the tensile strength. Hoang (2019) further showed that rotational disruption determines the maximum grain radius (or the upper cut-off of the grain size distribution), which depends on both the interstellar radiation field (ISRF) intensity and the grain tensile strength. Other than determining the upper cut-off of grain radii, rotational disruption could also enhance the small grain production. Thus, for a complete understanding of the grain size distributions in galaxies, we should clarify how rotational disruption affects the evolution of grain size.

Since rotational disruption is more efficient in higher ISRFs, it is more important in starburst (or actively star-forming) galaxies. The dust temperature which reflects the ISRF intensity is generally high in those galaxies (e.g. Zavala et al. 2018). Starburst galaxies emit most of their stellar radiation energy by dust emission (Sanders & Mirabel 1996), which means that understanding dust properties is crucial in clarifying the radiative processes in those galaxies. In addition, the fraction of stellar light reprocessed by dust increases towards $z \sim 1-2$, when the cosmic star formation rate is the highest (e.g. Takeuchi et al. 2005b; Goto et al. 2010; Burgarella et al. 2013). In such dusty star-forming galaxies, rotational disruption could play a significant role in determining the dust properties through the modification of grain size distribution.

The goal of this paper is to clarify the effect of rotational disruption on the evolution of grain size distribution. As a representative quantity that reflects the grain size distribution, we also calculate extinction curves. In our previous modelling, shattering was the unique process that produces small grains, but the shattering rate might be uncertain because of the assumed grain velocities. In this paper, we treat rotational disruption as *an alternative mechanism of small-grain production* (i.e. we examine the case where rotational disruption is the dominant mechanism of creating small grains from large grains). This step also serves to

provide a means of testing the role of rotational disruption against the observed dust properties.

To this goal, we newly formulate and include the effect of rotational disruption in the framework that calculates the evolution of grain size distribution in a galaxy. The development of the framework is based on HM20, in which we also separated the grains into relevant species to calculate the extinction curve. This enables us to examine the effect of rotational disruption on the extinction curve as an observable signature. We also discuss the effects of a strong ISRF as expected for starburst galaxies and some high-redshift galaxies.

This paper is organized as follows. In Section 2, we describe the dust evolution model which treats the grain size distribution and the grain composition. In particular, we newly include the effect of rotational disruption on the grain size distribution. In Section 3, we show the results. In Section 4, we provide some extended discussions, especially, regarding the significance of rotational disruption in galaxies with high ISRF intensities. In Section 5, we give the conclusion of this paper.

2 MODEL

The main purpose of the modeling in this paper is to investigate rotational disruption as an alternative mechanism of shattering in producing small grains. For this purpose, we use and extend the framework developed in our previous papers (HM20, originally based on Hirashita & Aoyama 2019). We model the metal and dust enrichment in a galaxy, which is treated as a one-zone object. The evolution of grain size distribution is calculated in a manner consistent with dust enrichment and interstellar dust processing. We newly include the effect of rotational disruption. Shattering also has a similar effect on small-grain production; in this paper, in order to clarify the role of rotational disruption in small-grain production, we turn off shattering. In other words, we include rotational disruption as an alternative small-grain-production mechanism to shattering to examine if rotational disruption could play a significant role in reproducing the observed dust properties. This is also equivalent to the assumption that rotational disruption is the dominant small-grain production mechanism over shattering. Turning off shattering also serves to obtain results not affected by the uncertainty in shattering (mainly caused by the assumed turbulence model). The case where rotational disruption and shattering coexist is discussed separately in Section 4.4.

The grain size distribution is further decomposed into silicate and carbonaceous dust; the latter species is further separated into aromatic and non-aromatic components. Distinction among the grain species is based on HM20 and is necessary to calculate the extinction curve. The infrared SED of dust emission could also be a useful output; however, since the calculation requires a consistent treatment of extinction curves and radiation transfer effects, the infrared SED is left for a future work. We only describe the outline of the models, and refer the interested reader to HM20 and Hirashita & Aoyama (2019) for details.

2.1 Evolution of grain size distribution

We assume the galaxy to be a closed box; that is, the galaxy starts its evolution with a certain mass of gas with zero metallicity and converts the gas to stars with the total baryonic (gas + stars) mass conserved. We adopt the following simple functional form for the star formation rate, ψ :¹

$$\psi(t) = \frac{M_{\text{g},0}}{\tau_{\text{SF}}} \exp\left(-\frac{t}{\tau_{\text{SF}}}\right), \quad (1)$$

where $M_{\text{g},0}$ is the initial gas mass (= total baryonic mass) and τ_{SF} is the star formation time-scale given as a free parameter. Using a set of equations that describe the chemical evolution of the galaxy, we obtain the time evolution of the masses of gas, stars, and metals, denoted as M_{gas} , M_{\star} , and M_{Z} , respectively. Because of the above assumption of closed box, $M_{\text{gas}} + M_{\star} = M_{\text{g},0}$ ($M_{\star} = 0$ at $t = 0$). The most important quantity that is calculated by this chemical evolution framework is the metallicity $Z \equiv M_{\text{Z}}/M_{\text{gas}}$. We also compute the silicon and carbon abundances (relative to the total gas mass), which are denoted as Z_{Si} and Z_{C} , respectively. In calculating the abundances of metals, silicon and carbon, we adopt the stellar yields in the literature (see HM20 for the references). We also need the SN rate (denoted as γ), which is calculated by assuming that stars in a zero-age-main-sequence mass range of 8–40 M_{\odot} become SNe at the end of their lives. We adopt the Chabrier initial mass function (Chabrier 2003) with a stellar mass range of 0.1–100 M_{\odot} .

We calculate the evolution of grain size distribution by considering the following processes: stellar dust production, dust destruction by SN shocks in the ISM, dust growth by accretion and grain–grain sticking by coagulation. As mentioned above, we turn off shattering to clarify the importance of small grain production by rotational disruption. We assume grains to be spherical and compact, so that the grain mass m is related to the grain radius a as $m = (4\pi/3)a^3s$, where s is the material density of dust. We adopt $s = 2.24 \text{ g cm}^{-3}$, which is appropriate for graphite (Weingartner & Draine 2001). As explained in HM20, our model is not able to include multiple dust components directly in the calculation of grain size distribution because of the difficulty in treating the interactions among various grain species. Thus, we adopt a ‘representative’ species for the grain size distribution, which is later separated into various species when we calculate the extinction curve. HM20 confirmed that the results are not sensitive to the adopted representative species. The grain size distribution at time t is expressed by the grain mass distribution $\rho_{\text{d}}(m, t)$, which is defined such that $\rho_{\text{d}}(m, t)dm$ is the mass density of dust grains whose mass is between m and $m + dm$. The grain size distribution, $n(a, t)$, is derived from the grain mass distribution as

$$\rho_{\text{d}}(m, t)dm = \frac{4}{3}\pi a^3 s n(a, t) da. \quad (2)$$

For dust processing, a multi-phase nature of the ISM is necessary to model. We assume that the ISM is composed of the diffuse (warm) and dense (cold) components, which have $(n_{\text{H}}/\text{cm}^{-3}, T_{\text{gas}}/\text{K}) = (0.3, 10^4)$ and $(300, 25)$, respectively (n_{H} is the hydrogen number density and T_{gas} is

the gas temperature). The mass fraction of the dense ISM is given as a constant parameter, η_{dense} . We calculate the change of grain mass distribution in a time-step interval Δt as $\Delta\rho_{\text{d}}(m, t) = [\partial\rho_{\text{d}}(m, t)/\partial t]_i f_i \Delta t$, where i indicates each process, $[\partial\rho_{\text{d}}(m, t)/\partial t]_i$ is the contribution from process i to the change of the grain mass distribution per unit time, and f_i is the fraction of the gas phase that hosts the process. The processes we consider are stellar dust production ($i = \text{star}$), SN destruction by sputtering ($i = \text{sput}$), dust growth by accretion ($i = \text{acc}$), and grain growth by coagulation ($i = \text{coag}$). We newly include rotational disruption ($i = \text{disr}$) in this paper. Stellar dust production and SN destruction are assumed to occur in both ISM phases, so that $f_{\text{star}} = f_{\text{sput}} = 1$. Coagulation and accretion take place only in the dense phase, so that $f_{\text{coag}} = f_{\text{acc}} = \eta_{\text{dense}}$. We also assume that rotational disruption occurs only in the diffuse ISM ($f_{\text{disr}} = 1 - \eta_{\text{dense}}$) for the following two reasons. First, the damping of grain rotation by sticking collision with gas particles is significant in the dense ISM (Hoang 2019). Secondly, the radiation could be effectively attenuated in the dense ISM. However, since rotational disruption takes place on a much shorter time-scale than the dust enrichment processes, the choice of f_{disr} does not affect our conclusions.

For the stellar dust production, we adopt the dust yields of SNe and AGB stars in the literature (see HM20 for the references). The dust mass supplied by the stellar sources are distributed in each grain radius bin based on the lognormal grain size distribution centered at 0.1 μm with standard deviation $\sigma = 0.47$ (Asano et al. 2013). Thus, in our model, we assume that stars produce large ($a \sim 0.1 \mu\text{m}$) grains (see HM20 for further arguments supporting this assumption).

The changes of grain size distribution by SN dust destruction and dust growth (accretion) are treated by taking the grain-size-dependent (or grain-mass-dependent) destruction and growth time-scales into account. The evolution of grain size distribution by these processes is described by an ‘advection’ equation in the grain-radius space (Hirashita & Aoyama 2019). The change of grain size distribution by coagulation is, on the other hand, described by the Smoluchowski equation. The grain–grain collision rates for various combinations of grain radii are evaluated based on the geometric cross-section and the turbulence-driven relative grain velocity (Ormel et al. 2009). The sticking efficiency is assumed to be unity. The evolution of grain size distribution by rotational disruption is also calculated as described in the next subsection.

2.2 Effect of rotational disruption

Rotational disruption causes fragmentation of grains by centrifugal force. The mechanism of disruption is common between rotational disruption and shattering in the sense that the internal stress exceeding the tensile strength is the cause of the disruption. Therefore, we expect that the grain size distribution is modified by rotational disruption in a way similar to shattering. Rotational disruption does not require grain–grain collisions, but occurs spontaneously on a time-scale (as a function of grain mass) $\tau_{\text{disr}}(m)$, which is evaluated later. The evolution of grain mass distribution by rotational

¹ In HM20, there is a typo for this equation.

disruption is described as

$$\left[\frac{\partial \rho_d(m, t)}{\partial t} \right]_{\text{disr}} = -\frac{\rho_d(m, t)}{\tau_{\text{disr}}(m)} + \int_0^\infty \frac{\rho_d(m_1, t)}{m_1 \tau_{\text{disr}}(m_1)} \theta_{\text{frag}}(m; m_1) dm_1, \quad (3)$$

where $\theta_{\text{frag}}(m; m_1)$ is the mass distribution function of fragments produced from a grain with mass m_1 . Although this equation can be derived for its own sake, it may be convenient to describe it in correspondence with the equation governing shattering as described in Appendix.

We adopt the following time-scale for rotational disruption from equation (32) of Hoang (2019):

$$\tau_{\text{disr}}(a) = 10^5 U^{-1} \left(\frac{S_{\text{max}}}{10^7 \text{ erg cm}^{-3}} \right)^{1/2} \left(\frac{a}{0.1 \mu\text{m}} \right)^{-0.7} \text{ yr} \quad (4)$$

for $a \geq a_{\text{disr}}$,

where U is the ISRF intensity normalized to the average value in the solar neighbourhood as given by Mathis et al. (1983), S_{max} is the tensile strength, and a_{disr} is the threshold grain radius for rotational disruption. We fixed the mean wavelength of the ISRF to $\bar{\lambda} = 0.5 \mu\text{m}$ in the original expression. For $a < a_{\text{disr}}$, no rotational disruption is assumed to occur (i.e. $\tau_{\text{disr}} = \infty$).

The threshold grain radius, a_{disr} , is estimated by Hoang (2019). We can use their equation (29), since the gas density and temperature of the diffuse ISM are in the regime where the damping of the grain rotation by the emission of IR photons is important. We also fix the radiation anisotropy degree to $\gamma_{\text{rad}} = 0.1$ and the mean ISRF wavelength to $\bar{\lambda} = 0.5 \mu\text{m}$, obtaining

$$\left(\frac{a_{\text{disr}}}{0.1 \mu\text{m}} \right)^{2.7} = 5.1 U^{-1/3} \left(\frac{S_{\text{max}}}{10^7 \text{ erg cm}^{-3}} \right)^{1/2}. \quad (5)$$

Note that this is valid for $a_{\text{disr}} \lesssim \bar{\lambda}/1.8 \simeq 0.28 \mu\text{m}$ (i.e. in the regime where the efficiency of radiative torque strongly depends on the grain radius). If a_{disr} is larger than $0.3 \mu\text{m}$, radiative torque cannot make the grain rotation fast enough to cause rotational disruption (Hoang 2019).

Finally, we determine the fragment mass distribution, $\theta_{\text{frag}}(m; m_1)$. Since there is no available physical model for the fragment mass distribution in rotational disruption, we use the fragment distribution function in shattering as a guide. The maximum and minimum masses of the fragments produced from a grain mass m_1 are assumed to be $m_{\text{f,max}} = 0.02m_1$ and $m_{\text{f,min}} = 10^{-6}m_{\text{f,max}}$, respectively (Guillet et al. 2011; Hirashita & Aoyama 2019). We adopt the following mass distribution function of fragments produced from a grain with mass m_1 :

$$\theta_{\text{frag}}(m; m_1) = \frac{(4 - \alpha_f)m_1 m^{(-\alpha_f+1)/3}}{3 \left[m_{\text{f,max}}^{4-\alpha_f} - m_{\text{f,min}}^{4-\alpha_f} \right]} \Phi(m; m_{\text{f,min}}, m_{\text{f,max}}), \quad (6)$$

where $\Phi(m; m_{\text{f,min}}, m_{\text{f,max}}) = 1$ if $m_{\text{f,min}} \leq m \leq m_{\text{f,max}}$, and 0 otherwise, and $\alpha_f = 3.3$ (Jones et al. 1996).

The above fragment mass distribution could be optimistic in the number of small fragments, but we basically adopt it to investigate a possibility of rotational disruption being an alternative to shattering for small-grain production. Formation of many small fragments in rotational disruption may be justified for inhomogeneous grains such as composite grains composed of tiny monomers and grains

covered by mantles. Such inhomogeneous structures generally contain many ‘interfaces’ with locally weak binding force. Since we are particularly interested in the disruption of highly inhomogeneous grains (with small tensile strength as explained in Section 2.4), it would be appropriate to consider the formation of many small fragments. We should also keep in mind that in the above, the whole disrupted grain is assumed to be fragmented without leaving a remnant. Thus, our model provides an optimistic case for the production of small grains also in this sense. We discuss the dependence on the fragment size distribution later in Section 4.2.

2.3 Calculation of extinction curve

As an observable quantity, we calculate the extinction curve. For this purpose, we decompose the grain size distribution into the relevant dust species. We adopt the same dust species as in HA20 for the convenience of comparison. The grain mass distributions of silicate (ρ_{sil}) and carbonaceous dust (ρ_{car}) are described by $\rho_{\text{sil}}(m, t) = f_{\text{sil}}(t)\rho_d(m, t)$, and $\rho_{\text{car}}(m, t) = [1 - f_{\text{sil}}(t)]\rho_d(m, t)$, respectively, where $f_{\text{sil}}(t)$ is the mass ratio of silicate to the total dust mass. The silicate fraction is calculated using the silicon-to-carbon abundance ratio calculated in the chemical evolution model in Section 2.1.

The carbonaceous grain size distribution is separated into aromatic and non-aromatic populations. We denote the grain mass distributions of the aromatic and non-aromatic species as $\rho_{\text{ar}}(m, t)$ and $\rho_{\text{non-ar}}(m, t)$, respectively, and introduce the aromatic fraction, which is defined as $f_{\text{ar}}(m, t) \equiv \rho_{\text{ar}}(m, t)/\rho_{\text{car}}(m, t)$. HA20 solved aromatization and aliphaticization, and showed that the aromatic fraction is $\simeq 1 - \eta_{\text{dense}}$ for most of the grain size range of interest. Therefore, we simply assume a constant aromatic fraction, $f_{\text{ar}} = 1 - \eta_{\text{dense}}$; that is, $\rho_{\text{ar}}(m, t) = (1 - \eta_{\text{dense}})\rho_{\text{car}}(m, t)$ and $\rho_{\text{non-ar}}(m, t) = \eta_{\text{dense}}\rho_{\text{car}}(m, t)$.

The extinction at wavelength λ in units of magnitude (A_λ) is calculated as

$$A_\lambda = (2.5 \log_{10} e) L \sum_j \int_0^\infty n_j(a) \pi a^2 Q_{\text{ext}}(a, \lambda), \quad (7)$$

where the subscript j indicates the grain species (i.e. silicate, aromatic carbon, and non-aromatic carbon), L is the path length, and $Q_{\text{ext}}(a, \lambda)$ is the extinction efficiency factor evaluated by using the Mie theory (Bohren & Huffman 1983). We use astronomical silicate (Weingartner & Draine 2001) for silicate, while we adopt graphite in the same paper for aromatic carbonaceous grains. For non-aromatic species, we adopt the optical constants of amorphous carbon taken from Zubko et al. (1996) (their ACAR) (see also Nozawa et al. 2015; Hou et al. 2016). HM20 also provided extinction curves calculated with different carbonaceous species; we only examine the above set of materials since it was successful in producing extinction curves similar to the Milky Way curve (in particular, the UV slope and the 2175 Å bump). The grain size distribution can be calculated by $n_j(a, t) = 3\rho_j(m, t)/a$ (see equation 2). The extinction is normalized to the value in the V band ($\lambda^{-1} = 1.8 \mu\text{m}^{-1}$); that is, we output A_λ/A_V , where L is cancelled out.

2.4 Variation of parameters

In this paper, we concentrate on the parameters that directly affect rotational disruption, i.e. U and S_{\max} . We fix the dense gas fraction ($\eta_{\text{dense}} = 0.5$) and the star formation time-scale ($\tau_{\text{SF}} = 5$ Gyr) unless otherwise stated. These values are appropriate for Milky Way-like galaxies (Nozawa et al. 2015).

The ISRF intensity U strongly depends on the star formation activity; however, it is also affected by the spatial dust distribution and the shielding of dust (i.e. by various radiation transfer effects). Since our one-zone model is not suitable for modeling radiation transfer, we simply treat U as a free parameter. We also neglect the spatial inhomogeneity in U and concentrate on the mean ISRF in the galaxy. Since rotational disruption occurs on a short time-scale, the local ISRF could be important. If the ISRF has a large variation within the galaxy, rotational disruption acts with different magnitudes among the places. Our one-zone treatment is not able to address this issue; thus, any effects that require spatially resolved treatments (such as the spatial and temporal inhomogeneity in the radiation field that dust grains experience) are left for a future work. This issue could be investigated by using radiation-hydrodynamic simulations that consistently solve the dust evolution (McKinnon et al. 2020). We emphasize that our simple treatment for U enables us to draw an explicit conclusion regarding the dependence on U , which could be useful for interpreting galaxies with known U (note that U can be estimated from the dust temperature; see Section 4.3). We mainly examine the range of $U \sim 1$ –100, which is appropriate for nearby galaxies (e.g. Hirashita & Ichikawa 2009), except for the starburst model discussed later.

For the tensile strength, the uncertainty is large because we only have limited knowledge on the grain structures. Note that the grains larger than a_{disr} are relevant here, since only grains with $a > a_{\text{disr}}$ are disrupted by rotational disruption. Therefore, to specify S_{\max} , we have to consider the tensile strength of large grains. Large grains could have complicated structures especially if they are formed after accretion and coagulation. Composite grains (composed of tiny monomers) typically have $S_{\max} \sim 10^7$ erg cm $^{-3}$, while compact grains have $S_{\max} \sim 10^9$ – 10^{11} erg cm $^{-3}$ (Hoang et al. 2019; Hoang 2019). A core-mantle interface is expected to have a tensile strength similar to composite grains. Since the grain properties are unknown, we simply survey a wide range of parameter for $S_{\max} \geq 10^7$ erg cm $^{-3}$.

3 RESULTS

3.1 Grain size distribution

We show the evolution of grain size distribution. We adopt $U = 1$ for the ‘fiducial’ case. To investigate the case where the effect of rotational disruption is the most prominently seen, we select a case of low tensile strength $S_{\max} = 10^7$ erg cm $^{-3}$, which is appropriate for composite grains and grain mantles. We show the results in Fig. 1a. We observe that, even at $t = 0.1$ Gyr, when the grain production is dominated by stellar sources, small grains are efficiently formed by rotational disruption. For comparison, we also show in Fig. 1b the evolution of grain size distribution without rotational disruption but including shattering following HM20.

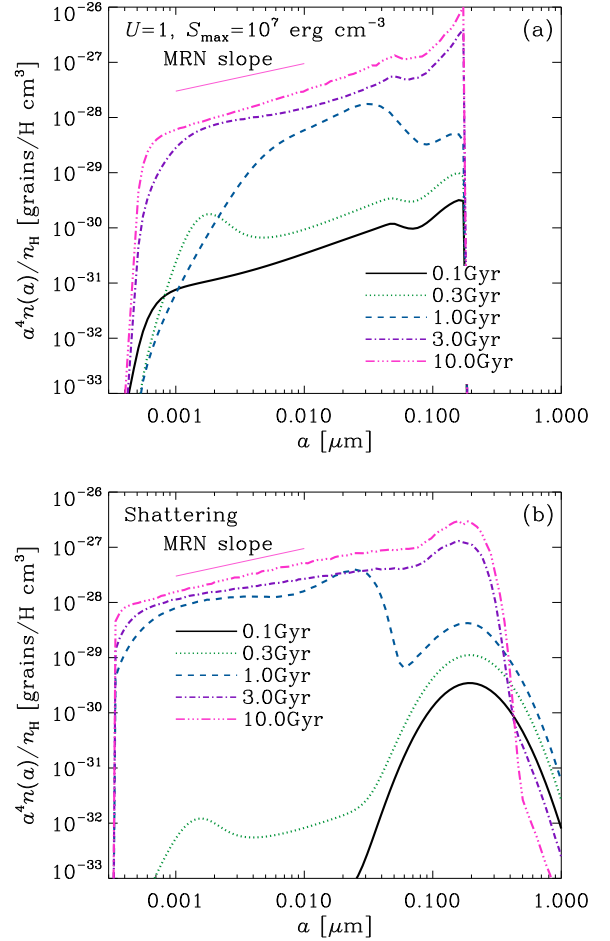


Figure 1. Evolution of grain size distribution. The grain size distribution is multiplied by a^4 and divided by n_{H} , so that the resulting quantity is proportional to the grain abundance per log a relative to the gas mass. We show the results (a) with rotational disruption and (b) with shattering instead of rotational disruption. The solid, dashed, dot-dashed, and triple-dot-dashed lines show the results at $t = 0.1, 0.3, 1, 3,$ and 10 Gyr, respectively. The thin dotted straight line shows the slope of the MRN grain size distribution ($n \propto a^{-3.5}$).

Since the efficiency of shattering depends on the dust abundance, the small-grain production is not prominent in the early stage ($t = 0.1$ Gyr). Thus, very different grain size distributions are predicted between rotational disruption and shattering in the early phase of galaxy evolution. At $t = 0.3$ Gyr, the bump at $a \sim 0.002$ μm is caused by accretion, and is seen in both panels. After $t \sim 3$ Gyr, the grain size distributions become smooth power-law-like forms, but there are some differences between rotational disruption and shattering. In the case with rotational disruption, there is a strong cut-off at $a = a_{\text{disr}}$ (note that $a_{\text{disr}} = 0.18$ μm for the current case), because the time-scale of rotational disruption is short. At $a < a_{\text{disr}}$, the grain size distribution is converged to a power-law-like shape but the overall slope is different: the scenario with rotational disruption predicts more large grains than that with shattering, since rotational disruption only occurs at $a > a_{\text{disr}}$. This is in contrast with shattering, in which small grains could also be fragmented if they

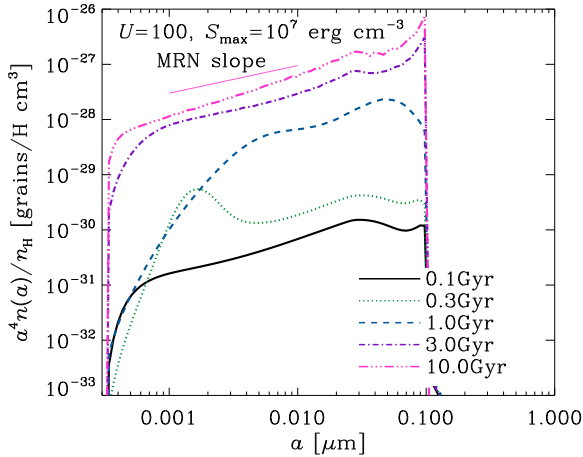


Figure 2. Same as Fig. 1a but for $U = 100$.

collide with large grains. As argued in HM20, the strong fragmentation cascade by shattering together with the grain growth by coagulation leads to an MRN-like grain size distribution with an overall slope of $p \approx 3.5$ ($n \propto a^{-p}$)² (see also Dohnanyi 1969; Williams & Wetherill 1994; Tanaka et al. 1996; Kobayashi & Tanaka 2010). However, rotational disruption cannot achieve this balance between fragmentation and coagulation because it does not occur at small grain radii. Less abundant small grains in rotational disruption lead to an overall slope p significantly smaller than 3.5.

We also examine the dependence on the parameters relevant for rotational disruption, that is, U and S_{\max} . First, we examine the effect of stronger radiation field by adopting $U = 100$ and $S_{\max} = 10^7$ erg cm⁻³. This case is expected to predict fast disruption with a small $a_{\text{disr}} (\approx 0.1 \mu\text{m})$. We observe in Fig. 2 [compared with Fig. 1(a)] that, if U is larger, the grain size distribution at $a \lesssim 0.003 \mu\text{m}$ is slightly more enhanced at $t \lesssim 0.3$ Gyr because of more efficient rotational disruption and accretion (which occurs predominantly at small grain radii). The enhancement of small grains in $U = 100$ leads to more efficient coagulation at $t = 1$ Gyr (as observed around $a \sim 0.05 \mu\text{m}$). The grain size distribution at $t \geq 3$ Gyr does not strongly depend on U , except for the smaller cut-off radius (a_{disr}) in the case of $U = 100$. Overall, the effects of a stronger ISRF appear in slight enhancement of small-grain production at early ages and a cut-off at smaller grain radii at all ages.

Next, we examine the dependence on S_{\max} . The above cases with $S_{\max} = 10^7$ erg cm⁻³ represent composite grains (or grain mantles) which are easy to disrupt. Here, we examine the cases for $S_{\max} = 10^8$ erg cm⁻³ with $U = 1$ ($a_{\text{disr}} = 0.28 \mu\text{m}$). This case is aimed at examining relatively inefficient rotational disruption. Note that if S_{\max} is larger than 10^8 erg cm⁻³, equation (5) is not applicable, since a_{disr} is larger than $0.28 \mu\text{m}$. This means that radiative torques cannot produce a grain rotation fast enough for rotational disruption. We observe in Fig. 3 that the effect of S_{\max} clearly appears in the maximum grain radii. The difference in S_{\max} is already apparent in the grain size distributions at $t \lesssim 0.3$

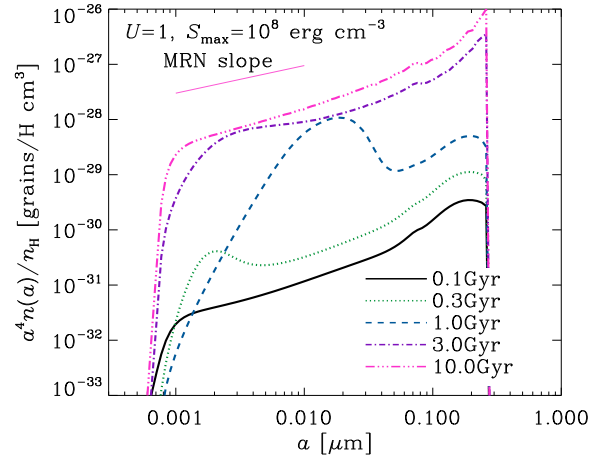


Figure 3. Same as Fig. 1 but for $S_{\max} = 10^8$ erg cm⁻³.

Gyr: small-grain production is less enhanced for larger S_{\max} because of less efficient rotational disruption. At $t \sim 1$ Gyr, the bump at $a \sim 0.01\text{--}0.03 \mu\text{m}$ is lower for large S_{\max} because less enhanced small-grain production leads to less efficient accretion. At later stages ($t \gtrsim 3$ Gyr), the grain mass distribution ($\propto a^4 n$) strongly peaks at $a = a_{\text{disr}}$. Therefore, rotational disruption not only determines the maximum grain radius but also govern the typical grain size at later ages.

3.2 Extinction curves

Based on the grain size distributions shown above, we calculate the extinction curves by the method explained in Section 2.3. In Fig. 4, we present the extinction curves corresponding to the grain size distributions shown in Fig. 1. We find that the extinction curve is overall steep in the case with rotational disruption in the earliest phases ($t \lesssim 0.3$ Gyr) because small grains are produced by rotational disruption on a short time-scale. Since the dust abundance is dominated by silicate, the 2175 Å bump is not prominent in the early stages. As a consequence, the extinction curve is similar to the Small Magellanic Cloud (SMC) extinction curve with rotational disruption. In contrast, the extinction curve is flat in the early epochs ($t \lesssim 0.3$ Gyr) with shattering, since shattering is not efficient enough to produce small grains when the dust abundance is small. In both cases, the extinction curve is the steepest at $t \sim 1$ Gyr, which corresponds to the epoch when accretion rapidly increases the abundance of small grains. The strength of the 2175 Å bump is weaker with rotational disruption than with shattering because the small-grain abundance is lower as seen in Fig. 1. At later epochs ($t \geq 3$ Gyr), the extinction curve is too flat to reproduce the Milky Way curve in the case with rotational disruption, while it is similar to the Milky Way curve in the case with shattering. This is because, as mentioned above, rotational disruption is less efficient at producing very small grains than shattering.

The effects of U and S_{\max} on the extinction curve are also examined. In Fig. 5, we show the extinction curves for higher U (with $S_{\max} = 10^7$ erg cm⁻³). Since we found that the extinction curves are sensitive to U , we examine $U = 3$ and 10 here. With stronger ISRF intensities, the grain size distri-

² Note that the slope is $(-p + 4)$ in the figure.

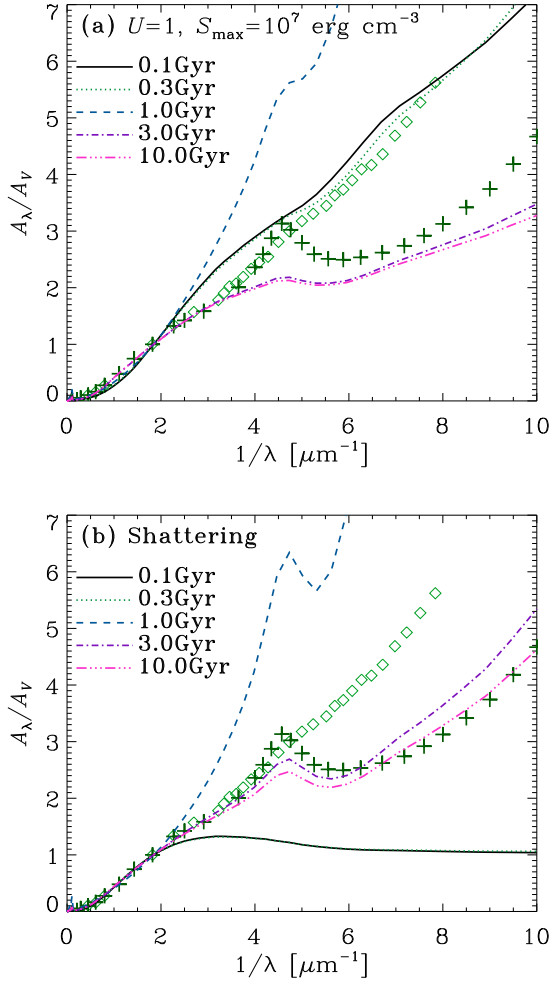


Figure 4. Extinction curves corresponding to the two cases shown in Fig. 1. Panels (a) and (b) show the results with rotational disruption and with shattering, respectively. The solid, dotted, dashed, dot-dashed, and triple-dot-dashed lines show the results at $t = 0.1, 0.3, 1, 3,$ and 10 Gyr, respectively. The lines at $t = 0.1$ and 0.3 Gyr are indistinguishable in panel (b). The crosses and diamonds show the observational data of the Milky Way and SMC extinction curves, respectively, taken from Pei (1992).

butions are steeper in the early stage of the evolution, even much steeper than the SMC extinction curve. This is mainly because of smaller cut-off radii for higher U ($a_{\text{disr}} = 0.16$ and $0.14 \mu\text{m}$ for $U = 3$ and 10 , respectively). Thus, if a galaxy has a higher ISRF intensity, we expect that the extinction curve is steeper in the early phase of galaxy evolution. At later epochs, the extinction curve is flattened; however, it is difficult to reproduce the Milky Way extinction curve. For $U = 3$, the carbon bump and UV slope are less prominent than the observed Milky Way curve. On the other hand, if we increase U further (as seen in the case of $U = 10$), the extinction curve become steeper, but they do not fit the Milky Way extinction curve because of the lack of large grains (i.e. a_{disr} is significantly smaller than the upper grain radius in MRN, $0.25 \mu\text{m}$). As shown by Nozawa & Fukugita (2013), the slope and the maximum grain radius of grain size dis-

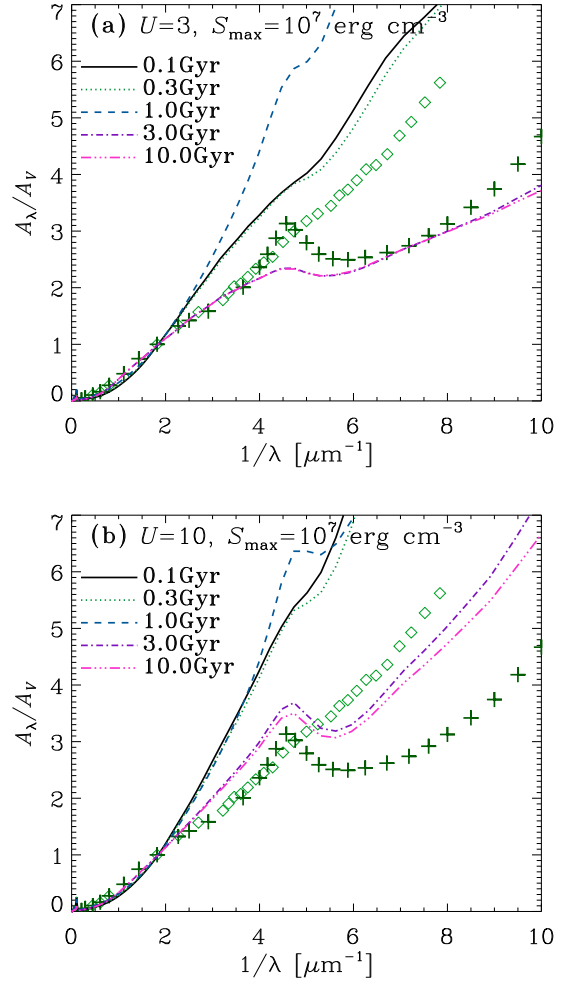


Figure 5. Same as Fig. 4a but for higher ISRF intensities [(a) $U = 3$ and (b) $U = 10$ (with $S_{\text{max}} = 10^7 \text{ erg cm}^{-3}$)].

tribution are both important to reproduce the Milky Way extinction curve.

We also show the extinction curves for higher $S_{\text{max}} (= 10^8 \text{ erg cm}^{-3})$ with $U = 1$ in Fig. 6 (the corresponding grain size distributions are shown in Fig. 3). With a higher tensile strength, the extinction curves are flat in the early stage of galaxy evolution because of larger $a_{\text{disr}} (= 0.28 \mu\text{m})$. Note that the steep extinction curve at $t = 1$ Gyr is due to accretion. Except for this short phase of efficient accretion, the extinction curves are generally flat for $S_{\text{max}} \geq 10^8 \text{ erg cm}^{-3}$. In other words, in order to produce extinction curves as steep as the SMC curves with rotational disruption, the tensile strength of large grains should be as small as expected for composites and grain mantles ($S_{\text{max}} \sim 10^7 \text{ erg cm}^{-3}$).

4 DISCUSSION

4.1 Rotational disruption compared with shattering

The time-scale of rotational disruption is typically shorter than that of chemical (dust) enrichment. Moreover, unlike

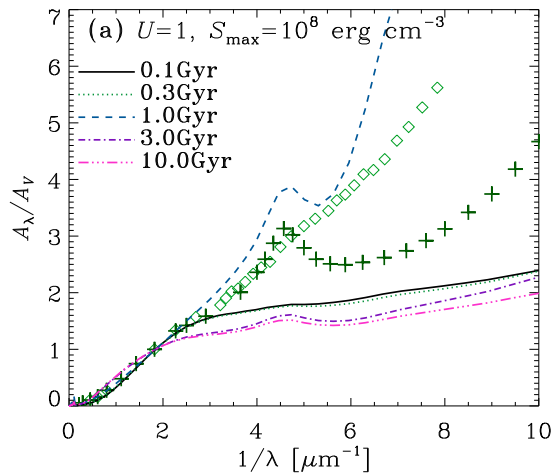


Figure 6. Same as Fig. 4a but for a higher tensile strength ($S_{\max} = 10^8 \text{ erg cm}^{-3}$ with $U = 1$).

shattering, the time-scale of rotational disruption is independent of the dust abundance. Therefore, the effect of rotational disruption appears even in the early stage of galaxy evolution. If the tensile strength is as low as expected for composites and grain mantles ($S_{\max} \sim 10^7 \text{ erg cm}^{-3}$), the threshold grain radius for rotational disruption is less than $0.2 \mu\text{m}$ even in the Milky Way ISRF ($U \sim 1$). Even though the dust supplied from stellar sources is dominated by large grains, efficient production of small grains by rotational disruption makes the grain size distribution completely different from the original log-normal shape (Fig. 1). Thus, rotational disruption provides a possible way of steepening extinction curves in the early stage of galaxy evolution. It is interesting to point out that, if rotational disruption is efficient, the SMC extinction curve is reproduced (Fig. 4). This is because the extinction curve becomes steep even in the early epoch when the carbon fraction is still low (note that graphite produces a prominent bump at 2175 \AA).

Although the above statement for the early phase of galaxy evolution is qualitatively robust, the extinction curves qualitatively depends on the fragment grain size distribution. As commented in Section 2.2, the assumption that the fragment grain size distribution is similar to the case of shattering may be optimistic in the production of small grains, although it could be justified if the grain structures are strongly inhomogeneous (with grain mantles, grain monomers, etc.). However, if we are interested in the extinction curves down to $\lambda \sim 0.1 \mu\text{m}$, the above conclusions are not greatly affected as long as fragments as small as $a \sim \lambda/(2\pi) \sim 0.016 \mu\text{m}$ are formed. If the minimum fragment size is larger than this, the extinction curves are not as steep as predicted in this paper (but are still steeper than the case without rotational disruption).

In later ($t \gtrsim 3 \text{ Gyr}$) epochs, the extinction curves are rather flat since rotational disruption only fragments grains at $a > a_{\text{disr}}$. Therefore, the resulting grain size distribution has a value of p (characteristic slope) smaller than the MRN value (3.5). Even if we increase U to decrease a_{disr} , the Milky

Way extinction curve is hard to reproduce because of p significantly smaller than 3.5.

As shown above, rotational disruption affects the evolution of grain size distribution even with $U = 1$ if the tensile strength is as small as expected for composites or grain mantles ($S_{\max} \sim 10^7 \text{ erg cm}^{-3}$). For example, if large grains are formed by coagulation, it is expected that the grains are composed of many monomers, some of which may be bound loosely. However, if large grains originate from condensation in stellar ejecta, they likely have a compact structure. The requirement for S_{\max} is relaxed in high ISRF fields as shown later; that is, rotational disruption could efficiently produce small grains for a wide range of tensile strengths (or grain structures). Therefore, in the future, we need to develop a framework that treats the evolution of the following three physical components consistently: grain material properties (especially tensile strength), ISRF, and grain size distribution.

4.2 Robustness of the resulting grain size distributions

In the above, we have shown that, at later ages, the dust abundance is dominated by grains around $a \sim a_{\text{disr}}$ and that the overall slope p is smaller than 3.5. Here we examine if these characteristics are robust against the uncertainties in the model. Since the overall slope is determined by the balance between small- and large-grain productions by rotational disruption and coagulation, respectively, we change some parameters that could largely change these processes. We fix $U = 1$ and $S_{\max} = 10^7 \text{ erg cm}^{-3}$.

First, we modify rotational disruption in such a way that small-grain production is more efficient. This is most efficiently done in our framework by changing the slope of the fragment grain size distribution (α_f in equation 6). We change it to $\alpha_f = 4$, in which case the fragments have an equal mass in logarithmic grain radius intervals. This value of α_f is well out of the range suggested by Jones et al. (1996) ($\alpha_f = 3.0\text{--}3.4$), so that this choice of α_f provides an extreme case. Since the difference appears most prominently at later ages, we only show the result at $t = 10 \text{ Gyr}$. The grain size distributions and the extinction curves are compared between the cases with $\alpha_f = 3.3$ (i.e. the above calculation) and 4 in Fig. 7.

We observe in Fig. 7a (the solid and dotted lines) that the grain size distributions at $a \gtrsim 0.03 \mu\text{m}$ is robust against the change of α_f . The effect of α_f indeed appears at small grain radii. However, we should note that $\alpha_f = 4$ provides an extreme case in terms of small-grain production as mentioned above. Thus, it is worth noting that the grain mass distribution has a sharp rise just below the maximum radius (a_{disr}) even in this extreme case.

Since the accumulation of large grains could also be affected by coagulation, we also examine the case where the coagulation efficiency is reduced by lowering the sticking coefficient to 0.1 (we assumed unity above). In Fig. 7a, we observe that the weaker coagulation indeed enhances the grain abundance at $a \sim 0.001\text{--}0.01 \mu\text{m}$ but that the grain size distribution at $a \gtrsim 0.03 \mu\text{m}$ is little affected by the efficiency of coagulation. Therefore, the accumulation of grains at a just below a_{disr} is robust.

As mentioned in Section 2.2, our fragment distribution

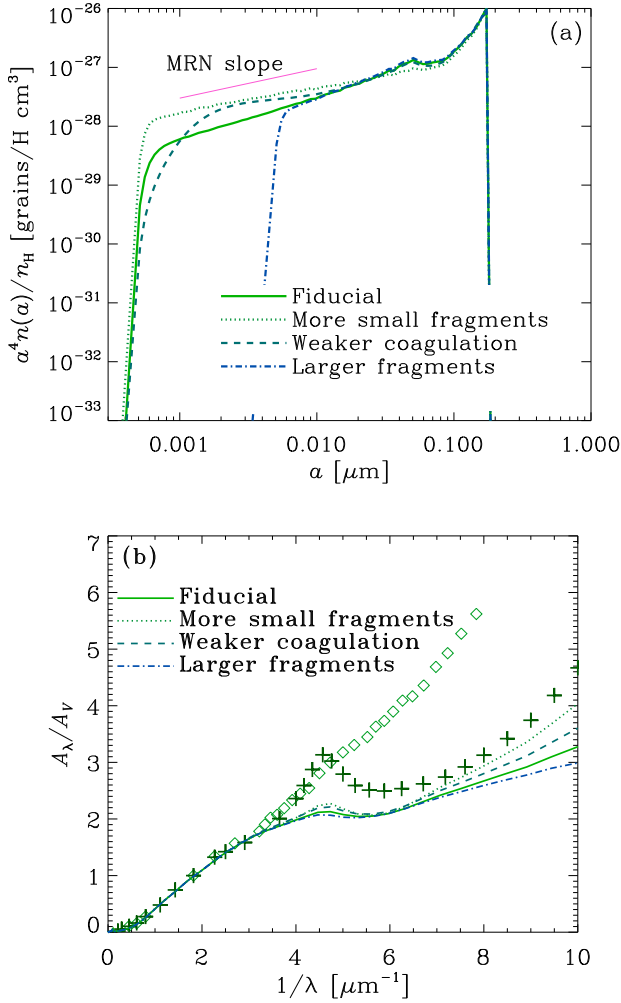


Figure 7. (a) Grain size distributions at $t = 10$ Gyr for different efficiencies of small-grain production by rotational disruption and large-grain production by coagulation. The fiducial case (i.e. the same case as in Fig. 1a), the case with $\alpha_f = 4$ (more small fragments in rotational disruption), the case with weaker coagulation (with a sticking efficiency of 0.1), and the case with a larger minimum fragment radius (10 times larger than the other cases) are shown by the solid, dotted, dashed, and dot-dashed lines, respectively. The thin short solid line shows the MRN slope for reference. (b) Extinction curves corresponding to panel (a). The line species are the same as in panel (a), and the Milky Way (crosses) and SMC (diamonds) extinction curves are shown for reference.

function may be optimistic in the abundance of small grains. We emphasize that even with this optimistic assumption, the dust mass is accumulated at grain radii just below a_{disr} . However, it is worth examining a less optimistic case, where the grains are fragmented into a much smaller number of pieces. In our model, this is easily done by making the minimum fragment mass larger. Here we adopt $m_{f,\text{min}} = 10^{-3} m_{f,\text{max}}$ instead of $m_{f,\text{min}} = 10^{-6} m_{f,\text{max}}$; that is, the minimum fragment size is 10 times larger than adopted in the above calculations. The grain size distribution at $t = 10$ Gyr is shown in Fig. 7. We observe that the grain size distribution is simply truncated at the smallest fragment radius ($a \sim 0.005 \mu\text{m}$). Thus,

we confirm that the minimum fragment size determines the minimum grain radius in our scenario.

We also show the extinction curves corresponding to the above grain size distributions in Fig. 7b. We observe that the extinction curves are not sensitive to α_f or the coagulation efficiency at $\lambda \gtrsim 0.15 \mu\text{m}$. The case with $\alpha_f = 4$ shows a significant steepening at far-UV because of the excess of grains at $a < 0.01\text{--}0.02 \mu\text{m}$ contributes to an excess of dust opacity at $\lambda < 2\pi a$. Therefore, the extinction curve shape at $\lambda \gtrsim 0.15 \mu\text{m}$ is robust against the enhancement of fragment production and the reduction of coagulation. It is natural that the extinction curve is flatter for the case with the larger $m_{f,\text{min}}$. However, the difference is not large since the minimum grain radius ($0.005 \mu\text{m}$) is still below $\lambda/(2\pi)$. If rotational disruption only produces grains larger than $0.016 \mu\text{m}$, the extinction curve is expected to be flattened significantly at $\lambda \sim 0.1 \mu\text{m}$.

In summary, the scenario in which small grains are predominantly produced by rotational disruption robustly predicts that the dust abundance is dominated by grains with $a \sim a_{\text{disr}}$ and that the overall slope of grain size distribution p is smaller than 3.5 at later ages. These properties of grain size distribution produce flat extinction curves; thus, it is difficult to explain the Milky Way extinction curve with a prominent carbon bump and a steep UV slope. Probably, shattering, which is turned off in our calculations, is still needed. However, this does not mean that rotational disruption is unimportant. We further discuss the importance of rotational disruption in the following subsections.

4.3 Parameter space where rotational disruption is important

The time-scale of rotational disruption is much shorter than that of galaxy evolution (chemical enrichment). This means that rotational disruption affects the grain size distribution in all the history of galaxy evolution. The most important factor in rotational disruption is the disruption radius a_{disr} , which determines the maximum grain radius. If we solve equation (5) for U , we obtain

$$U = 0.48 \left(\frac{a_{\text{disr}}}{0.2 \mu\text{m}} \right)^{-8.1} \left(\frac{S_{\text{max}}}{10^7 \text{ erg cm}^{-3}} \right)^{1.5}, \quad (8)$$

which can be regarded as an ISRF intensity that achieves a certain value of a_{disr} under a given tensile strength. In Fig. 8, we show the lines of $a_{\text{disr}} = 0.1, 0.2, \text{ and } 0.3 \mu\text{m}$ (the shaded areas show $a_{\text{disr}} < 0.1, 0.2, \text{ and } 0.3 \mu\text{m}$) on the U - S_{max} plane. We also convert U to the dust temperature (T_d) by adopting a scaling of $T_d = 18U^{1/6}$ K (since the dust temperature depends on the dust composition, we adopt the intermediate value between silicate and graphite; e.g. Li & Draine 2001). As mentioned above, rotational disruption occurs only if $a_{\text{disr}} \lesssim 0.28 \mu\text{m}$ (Section 2.2). Thus, we only show a_{disr} up to $0.3 \mu\text{m}$. This diagram gives us a clue to the significance of rotational disruption with observationally estimated T_d under an assumed grain tensile strength.

In Fig. 8, we observe that, for a tensile strength appropriate for composite grains ($S_{\text{max}} \sim 10^7 \text{ erg cm}^{-3}$), an ISRF intensity expected for normal star-forming galaxies (such as the Milky Way) is sufficient to destroy large ($a \gtrsim 0.2 \mu\text{m}$ ~ the upper grain radius of MRN) grains. For compact grains, which have $S_{\text{max}} \gtrsim 10^9 \text{ erg cm}^{-3}$, a strong ISRF ($U \gtrsim$ a few

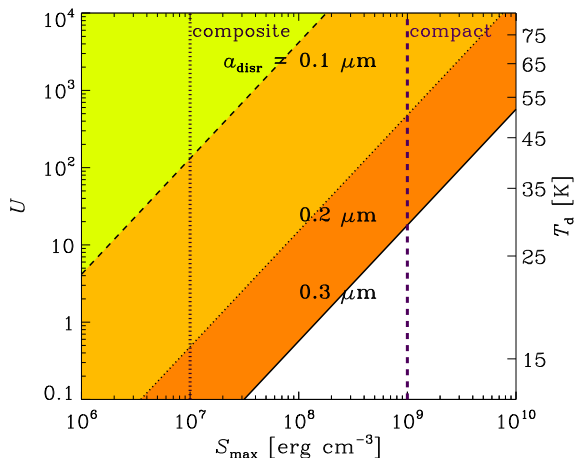


Figure 8. Constant a_{disr} lines on the U – S_{max} (ISRF–tensile strength) diagram. The diagonal solid, dotted, and dashed lines show $a_{\text{disr}} = 0.3$, 0.2 , and $0.1 \mu\text{m}$, respectively. The shaded areas present the regions where a_{disr} is smaller than those values. The tensile strengths discussed for composite and compact grains in the text are shown by the vertical dotted and dashed lines, respectively. The dust temperature corresponding to the ISRF intensity is shown on the right axis. In the white region, rotational disruption does not occur.

hundreds, or dust temperature $T_d \gtrsim 50$ K) is necessary to disrupt grains with $a \sim 0.2 \mu\text{m}$. With $U \sim 1$, rotational disruption is not capable of disrupting compact grains. Since the maximum grain radius in the Milky Way is $\approx 0.25 \mu\text{m}$ (MRN), rotational disruption is capable of determining the maximum grain radius only if the grains are much softer than compact grains.

4.4 Coexistence of rotational disruption and shattering

In this paper, in order to clarify the role of rotational disruption, we turned off the other small-grain production mechanism – shattering. In fact, the shattering efficiency also depends on the tensile strength (e.g. Tielens et al. 1994; Jones et al. 1996; Hirashita & Kobayashi 2013). If the tensile strength is as small as expected for composite grains or grain mantles, shattering would fragment almost all grains on the shattering time-scale ($\sim 10^8$ yr in solar-metallicity environment). However, such a small tensile strength may be applicable to only large grains, which are more likely to be composed of small monomers. In this case, both shattering and rotational disruption fragment large grains, determining the largest grain radius. Although rotational disruption only acts on large grains ($a > a_{\text{disr}}$), shattering still disrupts small grains even if they are compact. Thus, both rotational disruption and shattering affect large grains and contribute to determining the maximum size of grains, while shattering predominantly modifies the grain size distribution at $a < a_{\text{disr}}$.

The largest difference between rotational disruption and shattering is as follows: as mentioned above, the time-scale of the former process does not depend on the dust abundance while that of the latter does. This means that ro-

tational disruption could potentially be important even in the early phase of galaxy evolution. Indeed, it has been suggested (and it is also assumed in this paper) that dust grains formed by stellar sources is biased to large ($a \gtrsim 0.1 \mu\text{m}$) sizes. In the earliest phase of galaxy evolution, when dust is predominantly supplied by stellar sources, rotational disruption could be the only mechanism of producing small grains because shattering is inefficient in the condition of low dust abundance. We should keep in mind that a_{disr} strongly depends on the tensile strength; therefore, it is desirable to clarify the material properties of dust grains produced by stellar sources.

Although our knowledge on the grain-radius-dependent tensile strength is limited, it is possible to perform the following ‘experiment’ to illustrate a case where rotational disruption and shattering coexist (or ‘collaborate’). We simply calculate shattering based on the tensile strength appropriate for compact grains (here we assume graphite properties as adopted in Fig. 1b with a tensile strength of 4×10^{10} erg cm^{-3}) while we assume composite grains for rotational disruption ($S_{\text{max}} = 10^7$ erg cm^{-3}). This assumption could be justified since rotational disruption only affects large grains (which could be loosely bound as mentioned above) on a shorter time-scale than shattering. On the other hand, small grains are more likely to be compact so that shattering predominantly acts on compact grains.

In Fig. 9(a), we show the evolution of grain size distribution in the above setting of rotational disruption and shattering. We observe that rotational disruption clearly determines the sharp upper cut-off in the grain radius. The grain size distributions at young ages ($t \lesssim 0.3$ Gyr) is similar to the ones in Fig. 1(a), which means that shattering is inefficient in such young ages (because of low dust abundance). Therefore, we confirm that rotational disruption is a dominant small-grain-production mechanism over shattering in the early phase of galaxy evolution. Compared again with Fig. 1(a), at $t \gtrsim 1$ Gyr, more small grains are produced owing to shattering. In particular, the grain size distribution eventually shows a slope consistent with MRN ($p = 3.5$). Thus, the evolution of grain size distribution with shattering produces an MRN-like grain size distribution. In summary, if rotational disruption and shattering coexist, the upper limit of the grain radius is determined by rotational disruption throughout all ages, while the slope of grain size distribution converges to the MRN value at later ages if shattering is present.

We show the evolution of extinction curve in Fig. 9, which is to be compared with Fig. 4(a). As mentioned above, shattering is not important in the early phase of galaxy evolution; thus, the extinction curves at $t \leq 0.3$ Gyr is not modified by shattering. At later ages, small grains are efficiently produced by shattering and contribute to the steepening of extinction curve. Shattering is thus confirmed to be important in producing extinction curves as steep as the Milky Way curve. In summary, rotational disruption can predominantly shape the extinction curve in the early phase of galaxy evolution, while shattering could be necessary to explain an extinction curve as steep as the Milky Way curve at later ages.

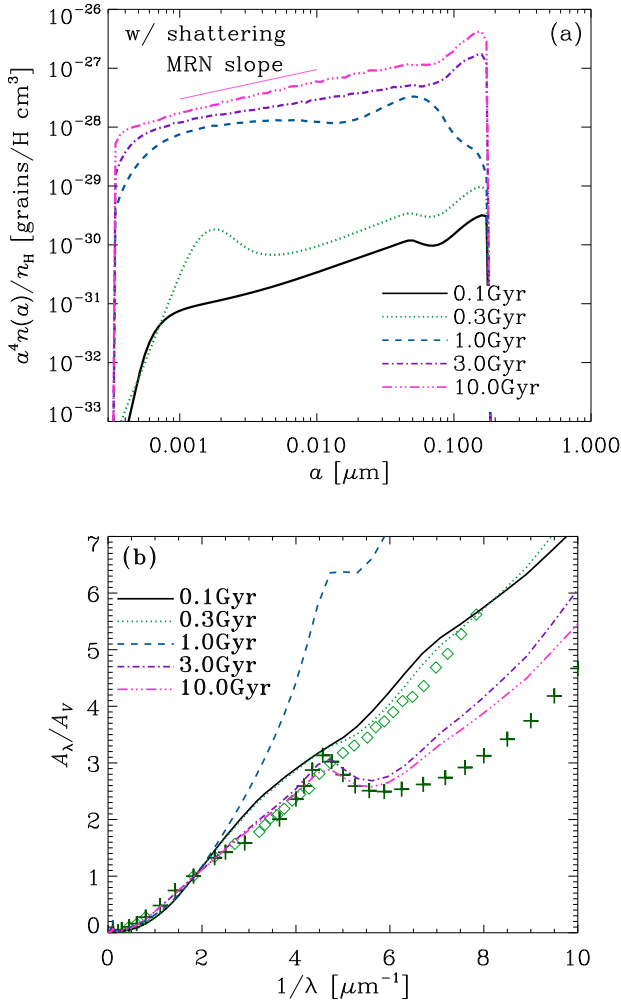


Figure 9. (a) Evolution of grain size distribution in the condition where rotational disruption and shattering coexist (see the text for the setting). The solid, dotted, dashed, dot-dashed, and triple-dot-dashed lines show the grain size distributions at $t = 0.1, 0.3, 1, 3,$ and 10 Gyr, respectively. The thin dotted line shows the MRN slope. (b) Evolution of extinction curve. The lines correspond to the same ages as in panel (a). The Milky Way (crosses) and SMC (diamonds) extinction curves are shown for reference.

4.5 Implication for starburst galaxies

In the above, we have fixed the star formation time-scale τ_{SF} to 5 Gyr. On the other hand, the typical star formation time-scale of starburst galaxies is a few $\times 10^8$ yr (e.g. Larson & Tinsley 1978). Starburst galaxies are interesting for rotational disruption because of their high ISRF environments. Following our previous paper, HM20, we adopt $\tau_{\text{SF}} = 0.5$ Gyr and $\eta_{\text{dense}} = 0.9$ to describe short star-formation time-scales and predominantly dense environments in starburst galaxies. This is referred to as the starburst model. We examine $U = 1000$ (corresponding to $T_d \sim 60$ K) for an extreme ISRF environment actually observed in starburst galaxies (e.g. Zavala et al. 2018; Lim et al. 2020). It is also interesting to examine a possibility of destroying compact grains, so that we examine $S_{\text{max}} = 10^9$ erg cm⁻³ as well as 10^7 erg cm⁻³.

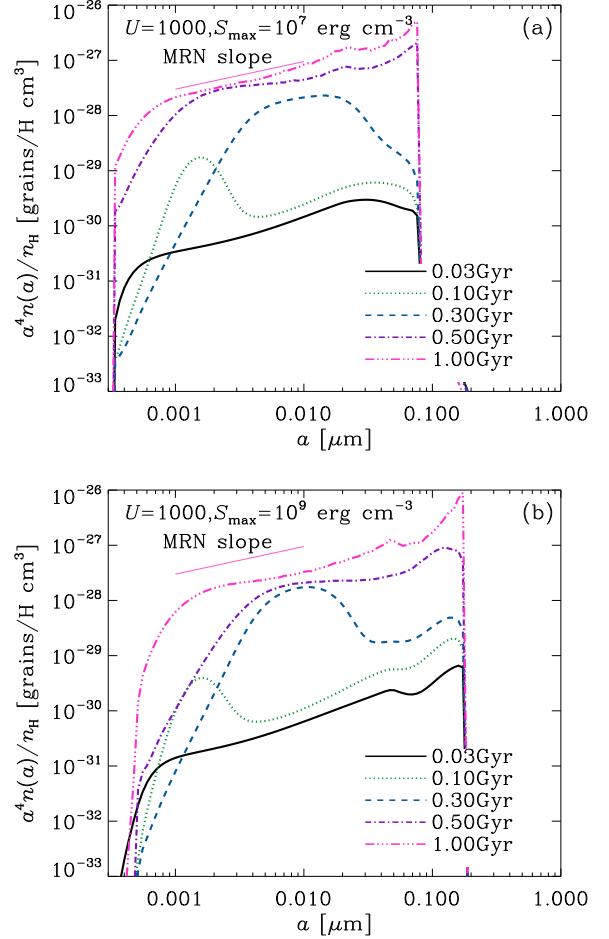


Figure 10. Evolution of grain size distribution for the starburst model (see the text). We adopt $S_{\text{max}} = 10^7$ and 10^9 erg cm⁻³ in panels (a) and (b), respectively, and fix $U = 1000$. The solid, dotted, dashed, dot-dashed, and triple-dot-dashed lines show the grain size distributions at $t = 0.03, 0.1, 0.3, 0.5,$ and 1 Gyr, respectively. The thin dotted line shows the MRN slope.

In Fig. 10, we show the resulting grain size distributions. Since the evolutionary time-scale is short, we show $t = 0.03, 0.1, 0.3, 0.5,$ and 1 Gyr. We observe that, except for the difference in the time-scale, the evolutionary behaviour of the grain size distribution is similar to that already investigated in Fig. 2. Small grains are abundant already at $t < 0.1$ Gyr because rotational disruption supplies small grains. Comparing the two panels in Fig. 10, the most prominent difference appears at the cut-off radius (a_{disr}). However, the grain size distribution at $a \ll a_{\text{disr}}$ is little affected by the difference in S_{max} . With the high value of $U = 1000$, even in the case of $S_{\text{max}} = 10^9$ erg cm⁻³, a_{disr} becomes smaller than $0.2 \mu\text{m}$.

In Fig. 11, we show the extinction curves corresponding to the above grain size distributions for the starburst models. We observe that the extinction curves stay steep for $S_{\text{max}} = 10^7$ erg cm⁻³ because of the small maximum grain radius (a_{disr}). Even for the harder-grain case of $S_{\text{max}} = 10^9$ erg cm⁻³, a significant steepening of extinction curve is seen even at $t < 0.1$ Gyr because of the efficient small-grain production by rotational disruption. It is interesting to point out that

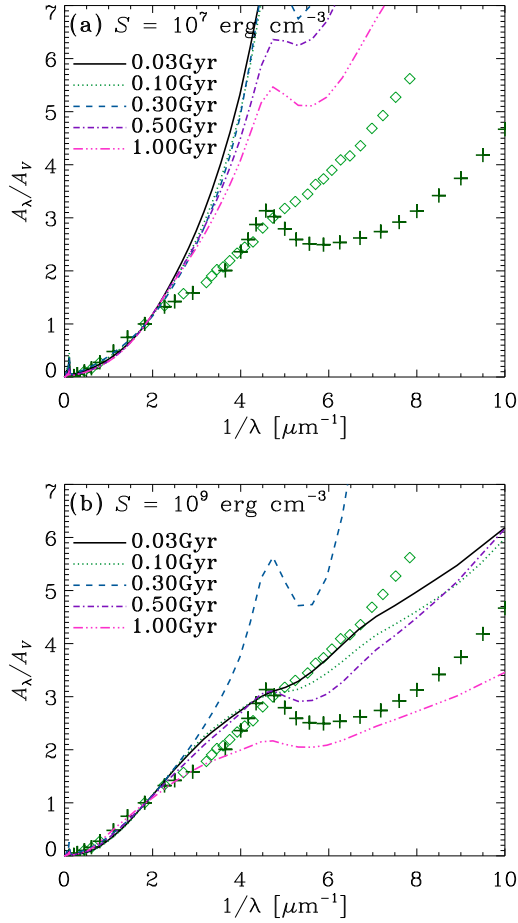


Figure 11. Evolution of extinction curve for the starburst model (see the text). Panels (a) and (b) present the results for the grain size distributions in the corresponding panels in Fig. 10. The line species for the ages are the same as in Fig. 10 (also shown in each panel).

the extinction curves are similar to the SMC curve at young ages. The extinction curves become flatter at later stages because of coagulation. Therefore, in starburst galaxies, the small-grain production by rotational disruption could put a significant imprint on the extinction curves especially at young ages.

For some starburst galaxies, attenuation curves, which include all the radiation transfer effects, are obtained instead of extinction curves (e.g. Calzetti 2001). The effects of dust distribution geometry and of stellar-age-dependent extinction make the attenuation curve significantly different from the original extinction curve (e.g. Witt & Gordon 2000; Inoue 2005; Seon & Draine 2016; Narayanan et al. 2018). Therefore, the fact that the extinction curves derived in this paper are different from the so-called Calzetti attenuation curve is not a contradiction. We leave radiation transfer calculations of attenuation curves and comparison with observations for future work.

4.6 Implication for high-redshift galaxies

The evolution of dust temperature along the redshift is still being debated. While there have been some observational indications that the dust temperature tends to be higher in higher redshift galaxies (Symeonidis et al. 2013; Béthermin et al. 2015; Schreiber et al. 2018; Zavala et al. 2018), the trend could be driven by an observational bias (Lim et al. 2020). At $z \gtrsim 5$, Lyman break galaxies (LBGs) and Lyman α emitters have dust temperatures typically higher than ~ 35 K, and some could have dust temperatures as high as $\gtrsim 70$ K (e.g. Hirashita et al. 2017; Bakx et al. 2020). Ferrara et al. (2017) also theoretically suggested that the dust temperature in the diffuse ISM of high-redshift LBGs could be as high as 35–60 K. These dust temperatures correspond to $U \sim$ a few tens to a few thousands. There are also some extreme populations of galaxies whose dust temperatures even reach ~ 90 K (Toba et al. 2020). This indicates that rotational disruption could have a significant imprint on the grain size distributions and the extinction curves in high-redshift galaxies.

Liu & Hirashita (2019) suggested that the extinction curves in high-redshift galaxies give us a clue to the dominant dust sources in the early Universe. Their dust evolution model did not include rotational disruption, so it predicted that the grains are biased to large sizes if the stellar dust production is dominant. However, if rotational disruption is as efficient as predicted by Hoang (2019) and this paper, small grains are abundant even if the dust production is dominated by stellar sources. Therefore, the steepness of extinction curve does not solely reflect the major dust sources. To isolate the effect of rotational disruption, it would be necessary to examine if the steepness of extinction curve has a correlation with the dust temperature (or ISRF intensity).

5 CONCLUSION

We formulate and calculate the evolution of grain size distribution in a galaxy by newly considering the effect of rotational disruption. We basically use the model developed in our previous papers but include rotational disruption instead of shattering for the major small-grain production mechanism. We evaluate the time-scale and grain radius threshold (above which grains are disrupted) by considering the dependence on the tensile strength of the grains and the ambient ISRF intensity (Hoang 2019).

We find that rotational disruption has a large influence on the evolution of grain size distribution in the following two aspects if the large grains are have a tensile strength $S_{\text{max}} \sim 10^7 \text{ erg cm}^{-3}$ as expected for composite grains and grain mantles. First, because of the short time-scale of rotational disruption, the small-grain production occurs even in the early stage of galaxy evolution, when the grain production is dominated by stellar sources. Therefore, even though stars produce large grains, rotational disruption enhances the abundance of small grains. As a consequence, the extinction curves could be as steep as the SMC extinction curve even in the early phase of galaxy evolution. Secondly, the upper bound of the grain radius is determined by the threshold of rotational disruption (a_{disr}). The steepness of extinction curve is basically regulated by a_{disr} at later epochs when interstellar processing dominates the grain size distribution.

For compact grains with $S_{\max} \gtrsim 10^9$ erg cm $^{-3}$, the grain size evolution is significantly affected by rotational disruption if the radiation field is as strong as expected for starburst galaxies ($U \gtrsim$ a few hundreds or $T_d \gtrsim 50$ K).

Rotational disruption differs from shattering in that it only occurs at the largest grain radii ($a > a_{\text{disr}}$). Therefore, we observe a concentration of grains around $a \sim a_{\text{disr}}$, and an overall slope shallower than the MRN value ($p < 3.5$). This produces too flat an extinction curve at later stages to reproduce the Milky Way extinction curve unless $a_{\text{disr}} \lesssim 0.1$ μm as expected in starburst galaxies. Rotational disruption tends to predict steep extinction curves for starburst galaxies.

If the ISRF is high in high-redshift galaxies as indicated by some observations, rotational disruption could play an important role in determining the grain size distributions in the early Universe. Thus, if the steepening of extinction curves in high-redshift galaxies is correlated with the dust temperature (or the ISRF intensity), we could argue that rotational disruption is really acting efficiently in the early stage of galaxy evolution.

ACKNOWLEDGEMENTS

We are grateful to the referee, K. Silsbee, for useful comments. HH thanks the Ministry of Science and Technology for support through grants MOST 107-2923-M-001-003-MY3 and MOST 108-2112-M-001-007-MY3 (RFBR 18-52-52006). TH acknowledges the support by the National Research Foundation of Korea (NRF) grants funded by the Korea government (MSIT) through the Basic Science Research Program (2017R1D1A1B03035359) and Mid-career Research Program (2019R1A2C1087045).

REFERENCES

- Aoyama S., Hirashita H., Nagamine K., 2020, *MNRAS*, **491**, 3844
 Asano R. S., Takeuchi T. T., Hirashita H., Nozawa T., 2013, *MNRAS*, **432**, 637
 Bakx T. J. L. C., et al., 2020, arXiv e-prints, p. arXiv:2001.02812
 Béthermin M., et al., 2015, *A&A*, **573**, A113
 Bohren C. F., Huffman D. R., 1983, *Absorption and Scattering of Light by Small Particles*. Wiley
 Burgarella D., et al., 2013, *A&A*, **554**, A70
 Calzetti D., 2001, *PASP*, **113**, 1449
 Cazaux S., Tielens A. G. G. M., 2004, *ApJ*, **604**, 222
 Chabrier G., 2003, *PASP*, **115**, 763
 Chen L.-H., Hirashita H., Hou K.-C., Aoyama S., Shimizu I., Nagamine K., 2018, *MNRAS*, **474**, 1545
 Dohnanyi J. S., 1969, *J. Geophys. Res.*, **74**, 2531
 Draine B. T., Weingartner J. C., 1996, *ApJ*, **470**, 551
 Ferrara A., Hirashita H., Ouchi M., Fujimoto S., 2017, *MNRAS*, **471**, 5018
 Goto T., et al., 2010, *A&A*, **514**, A6
 Gould R. J., Salpeter E. E., 1963, *ApJ*, **138**, 393
 Guillet V., Pineau Des Forêts G., Jones A. P., 2011, *A&A*, **527**, A123
 Hirashita H., Aoyama S., 2019, *MNRAS*, **482**, 2555
 Hirashita H., Harada N., 2017, *MNRAS*, **467**, 699
 Hirashita H., Ichikawa T. T., 2009, *MNRAS*, **396**, 500
 Hirashita H., Kobayashi H., 2013, *Earth, Planets, and Space*, **65**, 1083
 Hirashita H., Murga M. S., 2020, *MNRAS*, **492**, 3779

- Hirashita H., Burgarella D., Bouwens R. J., 2017, *MNRAS*, **472**, 4587
 Hoang T., 2019, *ApJ*, **876**, 13
 Hoang T., Lazarian A., 2008, *MNRAS*, **388**, 117
 Hoang T., Lazarian A., 2009, *ApJ*, **695**, 1457
 Hoang T., Tram L. N., Lee H., Ahn S.-H., 2019, *Nature Astronomy*, **3**, 766
 Hou K.-C., Hirashita H., Michałowski M. J., 2016, *PASJ*, **68**, 94
 Inoue A. K., 2005, *MNRAS*, **359**, 171
 Jones A. P., Tielens A. G. G. M., Hollenbach D. J., McKee C. F., 1994, *ApJ*, **433**, 797
 Jones A. P., Tielens A. G. G. M., Hollenbach D. J., 1996, *ApJ*, **469**, 740
 Kobayashi H., Tanaka H., 2010, *Icarus*, **206**, 735
 Larson R. B., Tinsley B. M., 1978, *ApJ*, **219**, 46
 Li A., Draine B. T., 2001, *ApJ*, **554**, 778
 Liffman K., Clayton D. D., 1989, *ApJ*, **340**, 853
 Lim C.-F., et al., 2020, *ApJ*, **889**, 80
 Liu H.-M., Hirashita H., 2019, *MNRAS*, **490**, 540
 Mathis J. S., Rumpl W., Nordsieck K. H., 1977, *ApJ*, **217**, 425
 Mathis J. S., Mezger P. G., Panagia N., 1983, *A&A*, **128**, 212
 McKinnon R., Vogelsberger M., Torrey P., Marinacci F., Kannan R., 2018, *MNRAS*, **478**, 2851
 McKinnon R., Kannan R., Vogelsberger M., O’Neil S., Torrey P., Li H., 2020, *MNRAS*, *submitted*, arXiv:1912.02825
 Narayanan D., Conroy C., Davé R., Johnson B. D., Popping G., 2018, *ApJ*, **869**, 70
 Nozawa T., Fukugita M., 2013, *ApJ*, **770**, 27
 Nozawa T., Asano R. S., Hirashita H., Takeuchi T. T., 2015, *MNRAS*, **447**, L16
 O’Donnell J. E., Mathis J. S., 1997, *ApJ*, **479**, 806
 Ormel C. W., Paszun D., Dominik C., Tielens A. G. G. M., 2009, *A&A*, **502**, 845
 Pei Y. C., 1992, *ApJ*, **395**, 130
 Rau S.-J., Hirashita H., Murga M., 2019, *MNRAS*, **489**, 5218
 Sanders D. B., Mirabel I. F., 1996, *ARA&A*, **34**, 749
 Schreiber C., Elbaz D., Pannella M., Ciesla L., Wang T., Franco M., 2018, *A&A*, **609**, A30
 Seok J. Y., Hirashita H., Asano R. S., 2014, *MNRAS*, **439**, 2186
 Seon K.-I., Draine B. T., 2016, *ApJ*, **833**, 201
 Symeonidis M., et al., 2013, *MNRAS*, **431**, 2317
 Takeuchi T. T., Ishii T. T., Nozawa T., Kozasa T., Hirashita H., 2005a, *MNRAS*, **362**, 592
 Takeuchi T. T., Buat V., Burgarella D., 2005b, *A&A*, **440**, L17
 Tanaka H., Inaba S., Nakazawa K., 1996, *Icarus*, **123**, 450
 Tielens A. G. G. M., McKee C. F., Seab C. G., Hollenbach D. J., 1994, *ApJ*, **431**, 321
 Toba Y., et al., 2020, *ApJ*, **889**, 76
 Weingartner J. C., Draine B. T., 2001, *ApJ*, **548**, 296
 Williams D. R., Wetherill G. W., 1994, *Icarus*, **107**, 117
 Witt A. N., Gordon K. D., 2000, *ApJ*, **528**, 799
 Yamasawa D., Habe A., Kozasa T., Nozawa T., Hirashita H., Umeda H., Nomoto K., 2011, *ApJ*, **735**, 44
 Zavala J. A., et al., 2018, *MNRAS*, **475**, 5585
 Zubko V. G., Mennella V., Colangeli L., Bussoletti E., 1996, *MNRAS*, **282**, 1321

APPENDIX A: ANALOGY BETWEEN SHATTERING AND ROTATIONAL DISRUPTION

Since both shattering and rotational disruption produce grain fragments, the equations describing them should have some similarity. Here, we make an attempt of deriving equation (3) from the shattering equation. Shattering is described

by the following equation in our model (HM20; developed from Jones et al. 1994, 1996):

$$\left[\frac{\partial \rho_d(m, t)}{\partial t} \right]_{\text{shat}} = -m \rho_d(m, t) \int_0^\infty \alpha(m_1, m) \rho_d(m_1, t) dm_1 + \int_0^\infty \int_0^\infty \alpha(m_1, m_2) \rho_d(m_1, t) \rho_d(m_2, t) \mu_{\text{shat}}(m; m_1, m_2) dm_1 dm_2, \quad (\text{A1})$$

where μ_{shat} describes the grain mass distribution function of the shattered fragments produced from a grain with mass m_1 in the collision with a grain with mass m_2 , and α is written as

$$\alpha(m_1, m_2) \equiv \frac{\sigma_{1,2} v_{1,2}}{m_1 m_2}, \quad (\text{A2})$$

where $\sigma_{1,2}$ and $v_{1,2}$ are the collisional cross-section and the relative velocity between the two colliding grains (with masses m_1 and m_2), respectively. We expect that, if we replace the grain–grain collision time-scale with the rotational disruption time-scale, we obtain the equation that describes rotational disruption. A grain with mass m experiences collisions on a time-scale of τ_{coll} , which is evaluated as

$$\tau_{\text{coll}}(m)^{-1} = m \int_0^\infty \alpha(m', m) \rho_d(m', t) dm'. \quad (\text{A3})$$

In rotational disruption, the grain m_1 spontaneously fragments; thus, the fragment mass distribution function does not depend on m_2 . Eventually, if we convert τ_{coll} to τ_{disr} and $\mu_{\text{shat}}(m; m_1, m_2)$ to $\theta_{\text{disr}}(m; m_1)$, we obtain the evolution of grain size distribution by rotational disruption (equation 3).

This paper has been typeset from a $\text{\TeX}/\text{\LaTeX}$ file prepared by the author.